



Experimental and numerical study of solidifying phase-change material in a triplex-tube heat exchanger with longitudinal/triangular fins

Ammar M. Abdulateef^{a,b,*}, Jasim Abdulateef^{a,b}, Sohif Mat^a, Kamaruzzaman Sopian^a, Bashir Elhub^a, Munther Abdullah Mussa^c

^a Solar Energy Research Institute, Universiti Kebangsaan Malaysia, 43600 Bangi, Selangor, Malaysia

^b Department of Mechanical Engineering, Diyala University, 32001, Diyala, Iraq

^c Department of Mechanical Engineering, Baghdad University, Baghdad, Iraq

ARTICLE INFO

Keywords:

Phase-change material
Triplex-tube heat exchanger
Triangular fins
Longitudinal fins
Solidification time

ABSTRACT

Latent heat thermal energy storage (LHTES) system uses a large triplex-tube heat exchanger (TTHX) with internal longitudinal fins incorporating phase-change material (PCM) was experimentally designed, tested, and evaluated. The PCM was entirely solidified using the both-sides freezing, as a main method under the influence of average discharging temperature was at 65 °C. The changes in the mass flow rates of 16.2, 29.4, and 37.5 min/kg were investigated. The solidification rate increased, as the mass flow rate increased, therefore the mass flow rate at 37.4 kg/min consumed a short time, compared with the 16.2 and 29.4 kg/min. Furthermore, the PCM completely solidified, as fast as at position B than position A from the entrance of the HTF-tube because of temperature variations in axial and angular direction during discharging process. Two types of extended surfaces, namely the longitudinal and triangular fins in various configuration were numerically studied. A significant enhancement was observed using internal, internal-external, and external triangular fins at 14%, 16%, and 18% respectively, compared to longitudinal fins configuration. Consequently, the external triangular finned tube has been considered the most efficient for the brief solidification PCM (630 min). The total energy released for the both types of fins were compared. The simulation results were agreed well with the experimental results.

1. Introduction

Solar energy is considered, as one of the most prospective sources of energy in many parts of the world. The characteristics of solar energy, such as being abundant and freely available, easily and directly utilizable, renewable and has continuity, and safe and environmentally friendly, make solar energy an attractive alternative to fossil fuels. However, the continuous increase in the level of greenhouse gas emissions and the depletion of fossil fuels are identified, as the main driving forces behind the efforts to effectively utilize different sources of renewable energy. Solar energy systems require thermal energy storage (TES) to eliminate the mismatch between energy supply and demand. Considerable emphasis is placed on continuous power generation during cloud transients and non-daylight hours for solar device applications.

Most phase-change materials (PCM) that are used, as storage media in TES systems suffer from a low thermal conductivity ($k \leq 0.2$ W/m K), which results in an incomplete melting and solidification process, and a significant temperature difference within the PCM that can cause

material failure and system overheating. Enhancing the thermal performance of TES systems is necessary in employing a PCM to various engineering applications, such as building heating, water heating, solar systems, electronic cooling, drying technology, refrigeration and cold storage, air conditioning, and waste heat recovery [1]. Furthermore, few attempts have been made to optimize the fin design for maximizing the performance of latent heat thermal energy storage (LHTES) systems. The fin design optimization presents two intrinsic difficulties. First, fin design optimization problems result in expensive computational costs. Second, an intrinsic difficulty emerges from the transient behavior of a PCM-LHTES system.

Many researchers studied the performances of different kinds of heat exchangers used in LHTES systems with a PCM, such as concentric-cylinder, shell and tube, and triplex-tube heat exchanger (TTHX), and their applications in melting and solidification process [2,3]. Abdulateef et al. [4] have reviewed geometric and design parameters of the various fins employed for enhancing thermal energy storage systems. Three configurations experimentally compared by Agyenim et al. [5], a concentric tube system with no fins and increased with circular, and

* Corresponding author.

E-mail address: ammarmohammed10@yahoo.com (A.M. Abdulateef).

Table 1
Thermos-physical properties of the PCM.

Properties	PCM (RT82)
Density, solid, ρ_s (kg/m ³)	950
Density, liquid, ρ_l (kg/m ³)	770
Specific heat, C_{pb} , C_{ps} (J/kg K)	2000
Latent heat of fusion, L (J/kg)	176,000
Dynamic viscosity, μ (kg/m s)	0.03499
Melting temperature, T_m (K)	350.15–358.15
Thermal conductivity, k (W/m K)	0.2
Thermal expansion coefficient (1/K)	0.001

Table 2
Latent heat of fusion and melting temperature of PCM (RT82) for 10 tests by DSC.

Test	Melting process			Solidification process		
	Onset point (°C)	Peak point (°C)	Heat of fusion (kJ/kg)	Onset point (°C)	Peak point (°C)	Heat of fusion (kJ/kg)
1	75.13	83.51	192.22	81.79	78.48	203.18
2	69.81	82.03	198.82	81.78	78.34	202.98
3	70.22	82.13	202.02	81.82	78.38	207
4	69.77	82.13	204.36	81.84	78.04	208.65
5	70.08	82.23	203.02	81.9	78.04	209.01
6	70.12	82.3	198.87	81.94	78.08	209.41
7	70.22	82.2	204.28	81.88	78.05	209.8
8	70.57	82.23	202.71	81.89	78.08	209.05
9	75.5	82.1	200.96	81.92	78.11	209.76
10	70.23	82.16	199.07	81.84	77.98	209.23
Average	71.165	82.302	200.633	81.86	78.158	207.807

longitudinal fins resulted in high efficiency at a minimum volume. The system with longitudinal fins showed the best performance with increasing thermal response of PCM during charging, and reduced sub-cooling during discharging. Abdulateef et al. [6] also simulated two types of extended surfaces, namely the longitudinal and triangular fins. A significant enhancement in PCM melting was accomplished using internal, internal-external, and external triangular fins at 11%, 12%, and 15% respectively, compared with the longitudinal fins cases. Experimentally, the PCM melting for both-sides heating was successfully achieved at 90 °C. However, the changes in the mass flow rates of 16.2, 29.4, and 37.4 min/kg on the PCM average temperature in the axial direction were investigated. Tay et al. [7] indicated the plain tubes, which contained the heat-transfer fluid (HTF) modified to accommodate the techniques of the pin and the circular fins attached to the tube. Comparisons were conducted based on the solidification process. The finned tube was found to yield better average effectiveness and shorter phase-change duration (25% faster in terms of the phase-change duration) because of the large heat-transfer area of the finned tube design, compared with the pinned tube. Manish and Jyotirmay [8] experimentally examined the enhancement in the heat-transfer for melting and solidification of the PCM in a shell and tube with three longitudinal fins installed on the HTF tube. Solomon and Velraj [9] experimentally studied the heat-transfer enhancement of the PCM used in free-cooling application during outward cylindrical solidification in a double pipe heat exchanger, in which the PCM was filled in the annulus along with eight longitudinal uniformly spaced copper fins of different heights and air, as the HTF passes through the inner tube. The solidification time was decreased because of the utilization of longitudinal fins. Castell et al. [10] conducted a solidification process in the LHTEs system with vertical external longitudinal fins. Heat-transfer enhancement achieves by the vertical fins on the HTF-side significantly promote the nature convection within the HTF. Celador et al. [11] presented

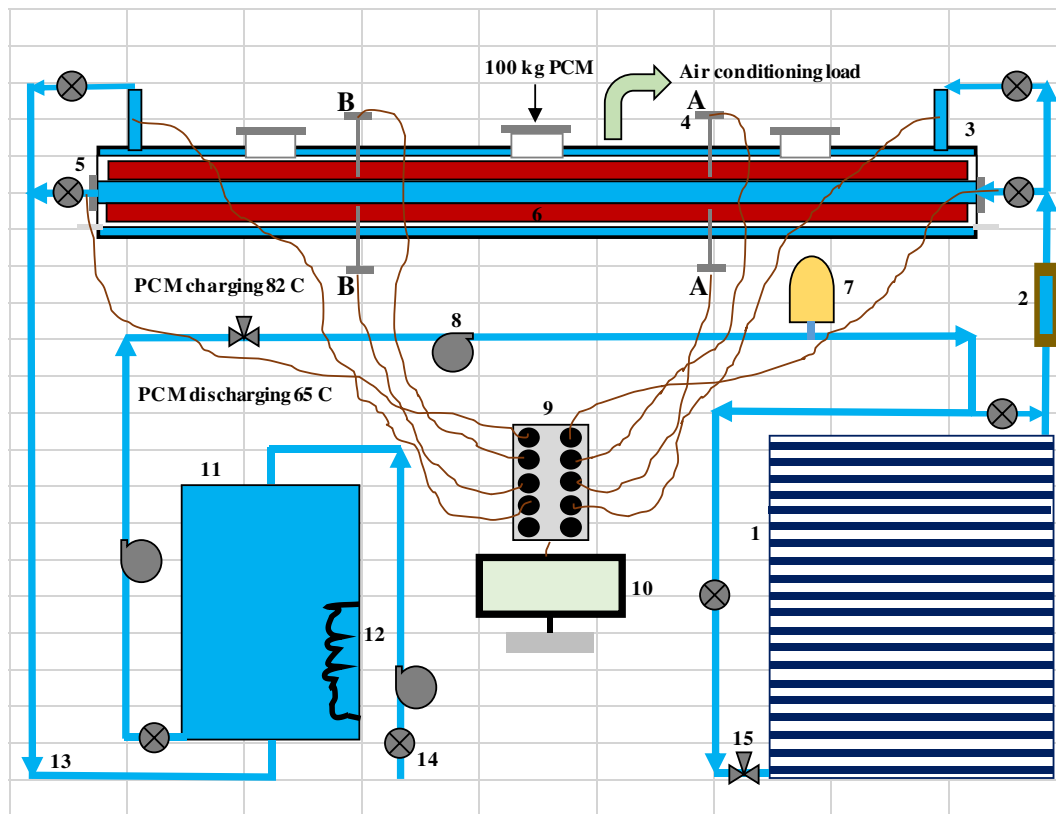


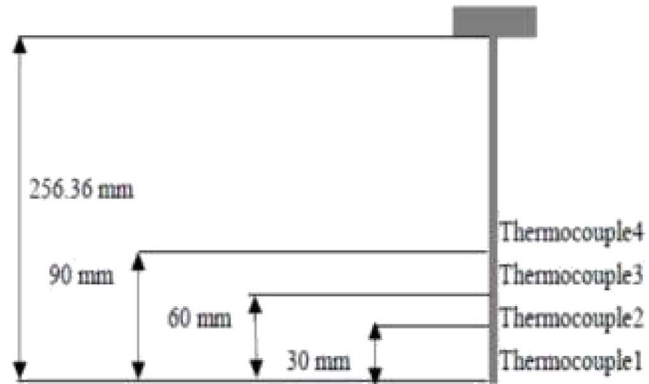
Fig. 1. Schematic of the experimental apparatus of the LHTEs system. It includes: 1. Evacuated tube solar collectors, 2. Flow meter, 3. TTHX, 4. T-type thermocouple, 5. J-type thermocouple (water), 6. Internal longitudinal fins, 7. Pressure vessel tank, 8. Pump, 9. Data logger, 10. Computer, 11. Water storage tank, 12. Electrical heater, 13. Pipes, 14. Valve two-ways, 15. Valve three-ways.



(a) TTHX



(b) T-type thermocouple



(c) Thermocouples arrangement

Fig. 2. TTHX with a T-type thermocouple.

three different modeling approaches, namely: numerical, simplified analytical, and simplified numerical approaches for an innovative finned plate in the LHTES system. Sciacovelli et al. [12] simulated the use of two kinds of tree shaped fins, namely: single and double bifurcation configurations, to optimize and achieve the maximum performance of PCM-LHTES system. Consequently, the longitudinal fins are the most common extended surfaces for enhancing the heat-transfer rate in LHTES systems. When a TTHX is used, the heat-transfer area can be directly augmented to the PCM surface, and the thermal performance is enhanced, compared with a cylinder or shell and tube heat exchanger.

This study presents the experimental and numerical investigations of the PCM solidification in a large TTHX with two types of extended surface (longitudinal and triangular fins). The triangular fin model has been simulated, as a unique extended surface to enhance the cooling rate between the PCM and the HTF, which contains fewer materials and may be more efficient than the familiar configurations of fins.

2. Experiments and procedures

2.1. Selection of PCM

The melting temperature of a PCM in the TES system, must match the operation range of the application. Akgun et al. [13] reported commercial-grade phase-change materials that exhibited stable properties after 1000 to 2000 cycles. Table 1 shows the selected RT82 paraffin (RUBITHERM GmbH-Germany), as a PCM with thermal properties (78.15 °C–82.15 °C, melting temperature) for our application. The system satisfies the minimum temperature requirement for air-conditioning systems, which is in the range of 65 °C–70 °C [14]. The properties, such as the latent heat of fusion (kJ/kg), melting temperature, and solidification temperature (°C), were measured using a differential scanning calorimetry (METTLER TOLEDO; Model DSC1). Approximately, 20 mg was used and repeated for 10 thermal cycling tests. The PCM was heated from 27 °C to 120 °C at a heating rate of 2 °C/min. The cooling process for PCM began from 120 °C to the ambient temperature under a cooling rate of 2 °C/min. Table 2 summarizes the results of physical properties tests.

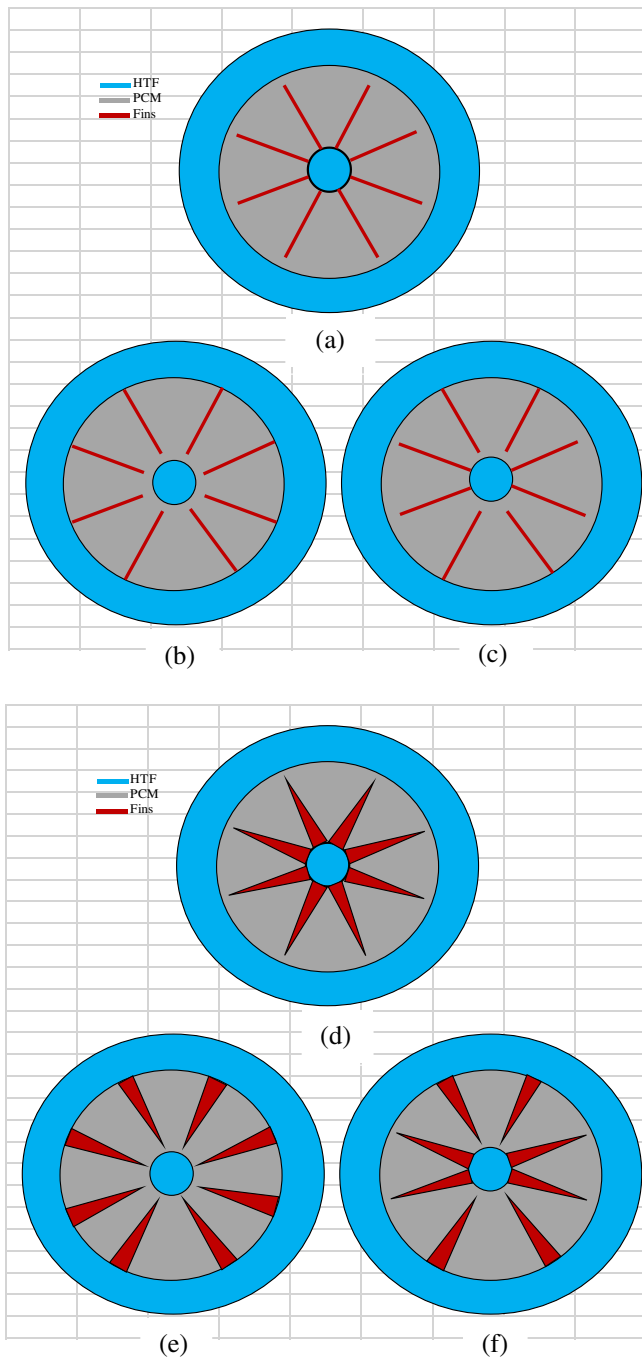


Fig. 3. Physical configurations of the TTHX models: (a) internal longitudinal fins, (b) external longitudinal fins, (c) internal-external longitudinal fins, (d) internal triangular fins, (e) external triangular fins, and (f) internal-external triangular fins.

2.2. Experimental apparatus

Fig. 1 shows the schematic of the LHTES experimental setup. The main items are included: evacuated tube solar collectors, a flow meter, a TTHX, J and T-type thermocouples, internal longitudinal fins, a pressure vessel tank, pumps, a water storage tank with an electrical heater, pipes with valves, a data logger, and a computer. TTHX is a major part in this system (see, Fig. 2a) and consists of inner, middle, and outer tubes with 76.2 mm, 381 mm, and 500 mm diameters with 3 mm thickness and 3000 mm length, respectively. Eight internal longitudinal fins were equally positioned and welded around the circumference of the inner tube at 45°. Each longitudinal fin has 121 mm

pitch, 2 mm thickness, and 2800 mm length. The inner and middle tubes and fins are made of copper, whereas the outer tube is made of steel. The inner and outer tubes were used for water as HTF, whereas the middle tube was filled in by 100 kg of the PCM. A 70-mm thick glass wool insulation ($k = 0.04 \text{ W/m K}$) was wrapped around the TTHX and pipes to decrease heat lost and to make the surface adiabatic. Fig. 2b and c show that two thermocouples on the top and bottom of the storage tank were fitted in the axial direction and were used to measure the temperatures of the PCM melting, 500 mm and 1100 mm away from the HTF-tube entrance, respectively. In addition, two thermocouples were installed at the inlet and outlet of the HTF-tube to measure the HTF inlet and outlet temperatures. The HTF flow rate was measured by a flow meter (measured at 3% accuracy) using T-type thermocouples (0.3% accuracy). The data recording for the discharging processes (PCM temperature and HTF mass flow rate) were achieved by a data logger and a personal computer.

2.3. Operation principle

After the PCM entirely charged, the discharging process starts. The water was circulated by the pumps from the water storage tank (500 L) to the TTHX. The valves were closed to prevent the water going to evacuated tube solar collectors, as shown in Fig. 1. The water followed by the HTF-convection to the inner and outer tubes of the TTHX and by the conduction to the PCM surface in the middle tube with inside, outside, and both-sides freezing method separately. The initial temperature of the PCM was set at 90 °C [6]. The inlet HTF was at average discharging temperature of 65 °C was continued to the TTHX during a closed cycle of the discharging process. The HTF-temperature cannot remain constant and continues to circulate until the PCM was completely solidified. Fig. 1 shows that valves were fixed in the pipes to control the operation. The LHTES system has been installed in the Green Technology Park at the Solar Energy Research Institute (SERI), Universiti Kebangsaan Malaysia (UKM).

3. Numerical approach

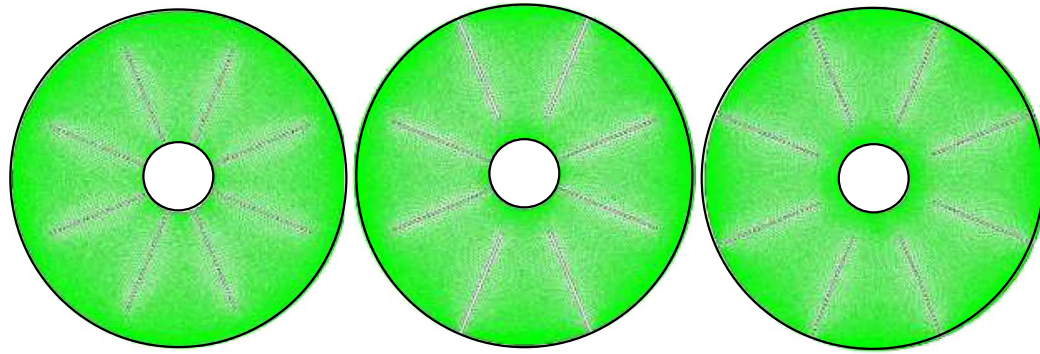
3.1. Physical models

The two physical configurations of the TTHX model were considered: (1) PCM-longitudinal fins and; (2) PCM-triangular fins, as shown in Fig. 3. The dimensions of the TTHX-longitudinal fins were the same for the TTHX-triangular fins, but the difference was in the base (thickness) of the triangular fin was at 25 mm. The internal, internal-external, and external configurations for longitudinal and triangular fins have been studied, as shown in Fig. 3. The heat-transfer during the PCM solidification process has been based on three freezing methods. For the both-sides freezing that uses as a main method, the cold water was supplied from both inner and outer tube during the discharging process. The minimum temperature required to operate the PCM-LHTES system was approximately 90 °C for the melting and 65 °C for solidification process, respectively.

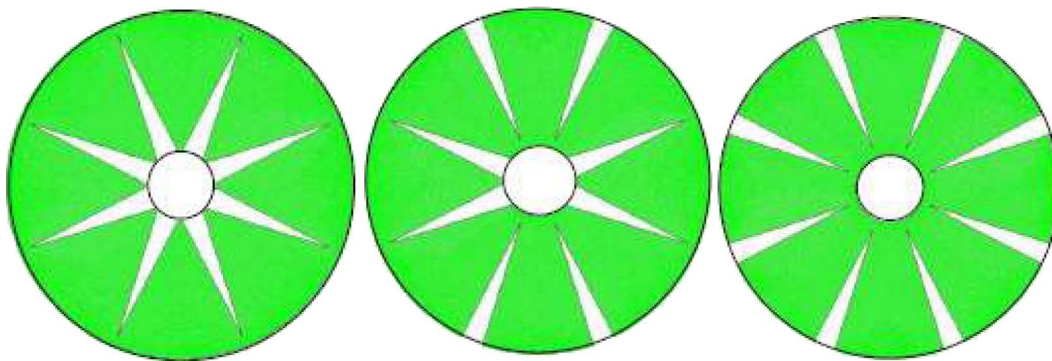
3.2. Governing equations

For the numerical analysis of the thermal process, the following assumptions were made: (1) the melting was Newtonian and incompressible; (2) the flow in the melting process was laminar and unsteady, with negligible viscous dissipations; (3) the thermophysical properties of the HTF and the PCM were independent of the temperature; (4) the heat-transfer was both conduction and convection-controlled. The three-dimensional convection is not considered, because a two-dimensional model is used.

The effect of natural convection during the melting and solidification process is considered by invoking the Boussinesq approximation, which is valid for the density variations of the buoyancy force;



(a) Internal longitudinal fins (b) Internal-external longitudinal fins (c) External longitudinal fins



(d) Internal triangular fins (e) Internal-external triangular fins (f) External triangular fins

Fig. 4. Distribution of the grids-size number in the middle tube of the TTHX-longitudinal fins and the TTHX-triangular fins.

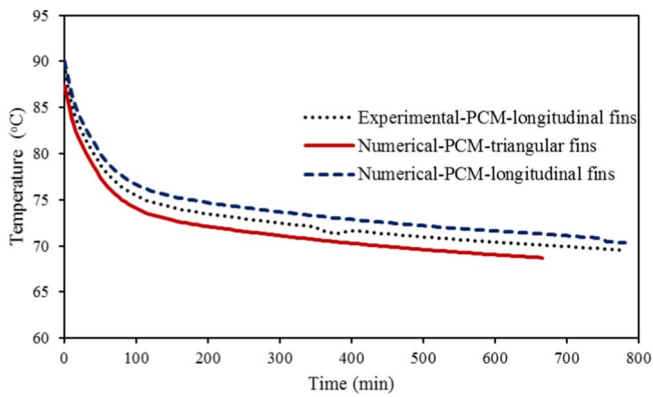


Fig. 5. Validation of the experimental and numerical model of the PCM in the TTHX-internal longitudinal fins and the TTHX-internal triangular fins.

otherwise, the effect is ignored. The density variation is defined, as follows:

$$\rho = \rho_l / (\beta(T - T_l) + 1) \tag{1}$$

where ρ_l is the PCM density at the melting temperature of T_l , and β is the thermal-expansion coefficient. The temperature distribution and viscous incompressible flow are solved by using the Navier-Stokes and thermal-energy equations, respectively. The continuity, momentum, and thermal energy equations are expressed, as follows [15].

The continuity equation:

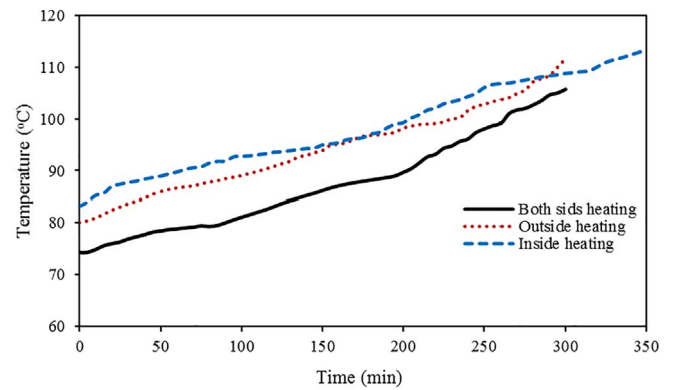


Fig. 6. The charging temperature versus time for three-heating methods with a flow rate of 37.5 kg/min.

$$\frac{\partial \rho}{\partial t} + \frac{\partial(\rho u)}{\partial x} + \frac{\partial(\rho v)}{\partial y} = 0 \tag{2}$$

The momentum equation:

$$\frac{\partial(\rho u)}{\partial t} + \frac{\partial(\rho u u)}{\partial x} + \frac{\partial(\rho v u)}{\partial y} = \frac{\partial}{\partial x} \left(\mu \frac{\partial u}{\partial x} \right) + \frac{\partial}{\partial y} \left(\mu \frac{\partial u}{\partial y} \right) - \frac{\partial p}{\partial x} + \rho g_x + S_x \tag{3a}$$

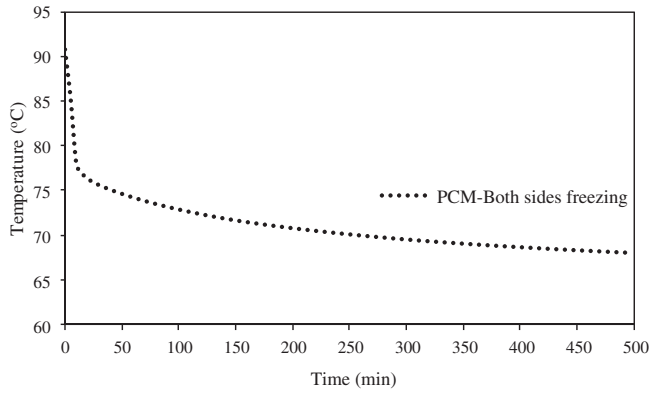


Fig. 7. Both-sides freezing method for solidifying the PCM with a flow rate of 37.5 kg/min.

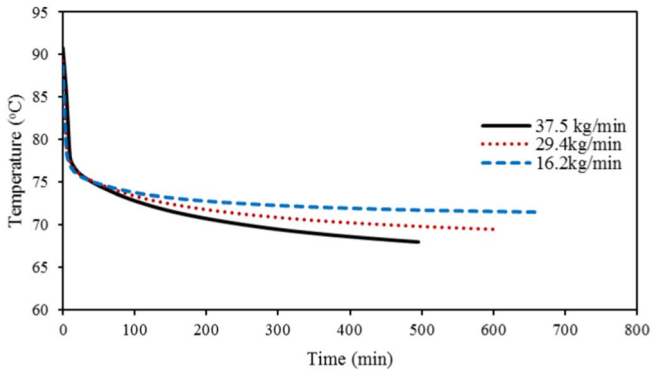


Fig. 8. The effects of mass flow rate by both-sides freezing on solidification of PCM ($T_i = 65^\circ\text{C}$).

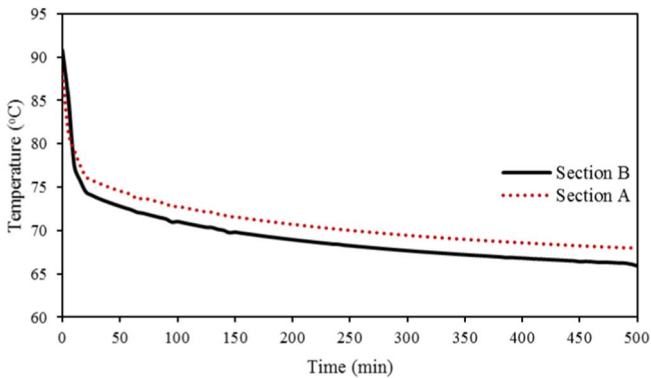


Fig. 9. The average temperature variation in the axial direction for both-sides freezing method ($T_i = 65^\circ\text{C}$).

$$\frac{\partial(\rho v)}{\partial t} + \frac{\partial(\rho uv)}{\partial x} + \frac{\partial(\rho v^2)}{\partial y} = \frac{\partial}{\partial x} \left(\mu \frac{\partial v}{\partial x} \right) + \frac{\partial}{\partial y} \left(\mu \frac{\partial v}{\partial y} \right) - \frac{\partial p}{\partial y} + \rho g_y + S_y \quad (3b)$$

The energy equation:

$$\frac{\partial(\rho h)}{\partial t} + \frac{\partial(\rho uh)}{\partial x} + \frac{\partial(\rho vh)}{\partial y} = \frac{\partial}{\partial x} \left(k \frac{\partial T}{\partial x} \right) + \frac{\partial}{\partial y} \left(k \frac{\partial T}{\partial y} \right) \quad (4)$$

where ρ is the density of the PCM, u and v are the fluid velocities, μ is the dynamic viscosity, p is the pressure, g is the gravitational acceleration, k is the thermal conductivity, h is the sensible enthalpy, and T is the temperature.

The sensible enthalpy equation can be written as follows:

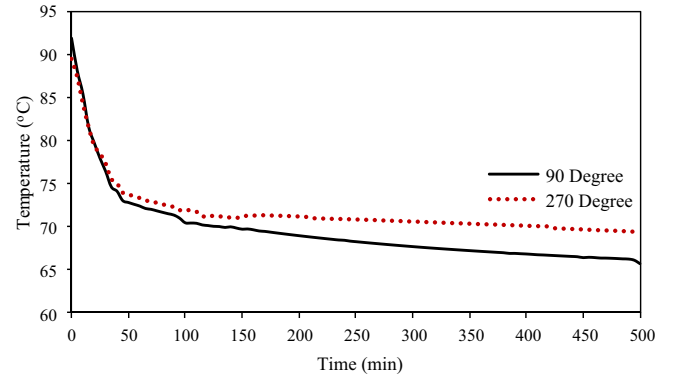


Fig. 10. The average temperature variation along the angular direction for both-sides freezing method ($T_i = 65^\circ\text{C}$).

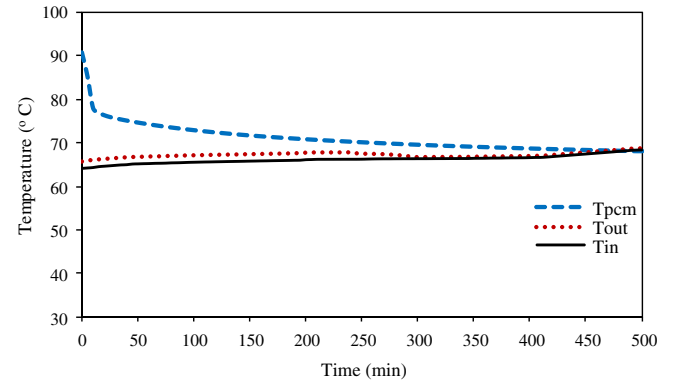


Fig. 11. The inlet and outlet discharging temperatures of the HTF, the average temperature of the PCM versus the time for the TTHX-longitudinal fins during the freezing process.

$$h = h_{ref} + \int_{T_{ref}}^T C_p \Delta T \quad (5)$$

where h_{ref} is the reference enthalpy at the reference temperature T_{ref} ; C_p is the specific heat.

The total enthalpy H equation can be defined as follows:

$$H = h + \Delta H \quad (6)$$

where ΔH is the latent heat content of the PCM; which changes between zero (solid) and L (liquid); and γ is the liquid fraction, which is generated during the phase-change between the solid and liquid states when the temperature is $T_i > T > T_s$. This can be written as:

$$\gamma = \Delta H / L \quad (7)$$

$$\gamma = 0 \quad \text{if } T < T_s$$

$$\gamma = 1 \quad \text{if } T > T_l$$

$$\gamma = \frac{T - T_s}{T_l - T_s} \quad \text{if } T_s < T < T_l \quad (8)$$

The source term S in the momentum equations, Eqs. (3a) and (3b) can be defined in x and y directions, respectively as:

$$S_x = C(1 - \gamma)^2 \frac{u}{\gamma^3 + \epsilon} \quad (9a)$$

$$S_y = C(1 - \gamma)^2 \frac{v}{\gamma^3 + \epsilon} \quad (9b)$$

where $C(1 - \gamma)^2 \frac{u}{\gamma^3 + \epsilon}$ and $C(1 - \gamma)^2 \frac{v}{\gamma^3 + \epsilon}$ are the ‘‘porosity function’’ defined by [16]. C is a constant, which describes how sharply the velocity is reduced to zero when the material solidifies. This constant varies between 10^4 and 10^7 (10^5 is considered for this paper). ϵ is a small number (0.001) to prevent division by zero.

Table 3
The new mean and the standard uncertainties of the PCM thermal properties.

Melting process			Solidification process		
Onset point (°C)	Peak point (°C)	Heat of fusion (kJ/kg)	Onset point (°C)	Peak point (°C)	Heat of fusion (kJ/kg)
70.1275 ± 0.148172	82.17625 ± 0.047953	201.64375 ± 1.386656	81.86 ± 0.02828	78.158 ± 0.090358	207.807 ± 1.359165

3.3. Boundary and initial conditions

The freezing process starts after the PCM entirely melted. At the initial time, the PCM was super-heat in the liquid state, and the temperature was 90 °C. The constant temperature of the tube wall represented the HTF temperature [17,18] and was approximately 65 °C. The boundary conditions of the TTHX can be written, as follows:

Both-sides freezing method:

$$\text{at } r = r_i \rightarrow T = T_{HTF} \quad (10)$$

$$\text{at } r = r_m \rightarrow T = T_{HTF} \quad (11)$$

Initial temperature of all models:

$$\text{at } t = 0 \rightarrow T = T_{ini} \quad (12)$$

3.4. Computational methodology

The PCM numerical model was solved using the software Ansys Fluent 15 via the enthalpy-porosity technique and the finite-volume method [19]. The model was drawn and meshed in two-dimensions (r , θ), and the boundary layers and zone types were defined using the software Gambit 2.4.6. Subsequently, the model was exported to the Fluent 15 software for solving the problem. The finite-volume method based on the transient time and pressure-based solver with absolute velocity in Fluent was used to solve the equations for the continuity, momentum, and energy, along with the boundary and initial conditions. The momentum and energy equations were discretized using the second-order upwind, and the pressure was discretized using the PRESTO method, which is the recommended approach for calculating natural convection flows. The SIMPLE scheme was employed in pressure-velocity coupling. The under-relaxation factors were 0.3, 0.2, 0.7, 1, and 0.9 for the pressure, velocity, momentum, energy, and liquid fraction, respectively. The convergence for the energy equation was 10^{-6} , and those for the velocity equations were 10^{-3} . The grid sizes of the numerical model for the internal, internal-external, and external longitudinal fins were calculated to be between 56,200 and 57,200, and to be between 66,536 and 64,633 for the internal, internal-external, and external triangular fins respectively, as illustrated in Fig. 4. For the time-step sensitivity, the data at 0.1 s was selected, as the standard value, and the measurements were performed at 0.5 and 1 s. Further details on the application of the LHTES system in computational fluid dynamics can be found in [20].

3.5. Numerical model validation

The present numerical models that were created using Gambit and Fluent 15 were experimentally validated for the PCM-internal longitudinal fins in TTHX, as shown in Fig. 5. For the two cases, the early stage of the solidification process represents the sensible cooling of the PCM, as a liquid. With time, the experimental results showed close agreement with the numerical results for the PCM-longitudinal fins based on the four thermocouples embedded into the PCM and the thermal loss that may be occurred in the experimental work, while the numerical results depended on the whole section of the model. The percentage errors between the numerical and experimental results did not exceed 3%, showing good agreement for PCM-longitudinal fins. Moreover, a good agreement was also seen between the PCM-triangular

fins and the PCM-longitudinal fins with percentage errors between their numerical results not exceeding 3.5%, as shown in Fig. 5. The average temperature of the PCM was 90 °C when the solidification process starts, and the HTF discharging temperature for both-sides freezing method was 65 °C with an experimental mass flow rate of 37.5 kg/min.

4. Results and discussion

Embedding fins in the PCM is an excellent technique for heat-transfer enhancement because of its simplicity, easy fabrication, and low construction cost [6]. The influences of the longitudinal fins based on both-sides freezing method in a large TTHX were experimentally investigated. The effects of the longitudinal and triangular fins welded to the inside, outside, and both-sides of the middle tube on the PCM solidification time were also numerically analyzed.

4.1. Experimental results

4.1.1. Average charging and discharging temperature

Fig. 6 illustrates the charging temperature versus time for three heating methods with a flow rate of 37.5 kg/min. Three heating methods were used for PCM charging included: inside, outside, and both-sides heating method, in which the average temperatures were 97 °C, 96 °C, and 90 °C, respectively. The charging temperature varied with time because of the intermitted nature of solar irradiance and should be not lower than the PCM melting temperature (82 °C) to achieve melting. The average temperature of the PCM was higher for both-sides heating than those in the inside and outside heating methods, whereas the charging temperature was the lowest among all methods at 90 °C because of the supply hot water from both-sides of the tube. After the PCM entirely charged, the discharging process starts until the PCM fully solidified at an average discharging temperature of 65 °C.

4.1.2. Both-sides freezing process

Several experiments were studied for solidifying the PCM in TES systems by applying the three freezing methods: inside, outside, and both-sides freezing method [5,14]. The major method used in this study was both-sides freezing method, where the cold water was supplied from the inner and outer tubes of the TTHX, in which an average discharging temperature supplied to the PCM by heat-conduction was at 65 °C. Fig. 7 shows both-sides freezing method for solidification of PCM with a flow rate of 37.5 kg/min. The temperature readings of PCM depended on T-type thermocouples (0.3% accuracy) location, as shown in Figs. 1 and 2.

4.1.3. The effect of the HTF mass flow rate

The effect of mass flow rate on the PCM solidification for both-sides freezing method was investigated based on the change in mass flow rate of 16.2, 29.4, and 37.4 min/kg, as shown in Fig. 8. The solidification rate increased, as the mass flow rate increased that caused decreasing the solidification time. That's because of the cooling rate reduced with time, because of the increase in the thermal resistance owing to the increase in the solid layer front. The PCM was completely solidified in shorter time at mass flow rate of 37.4 min/kg.

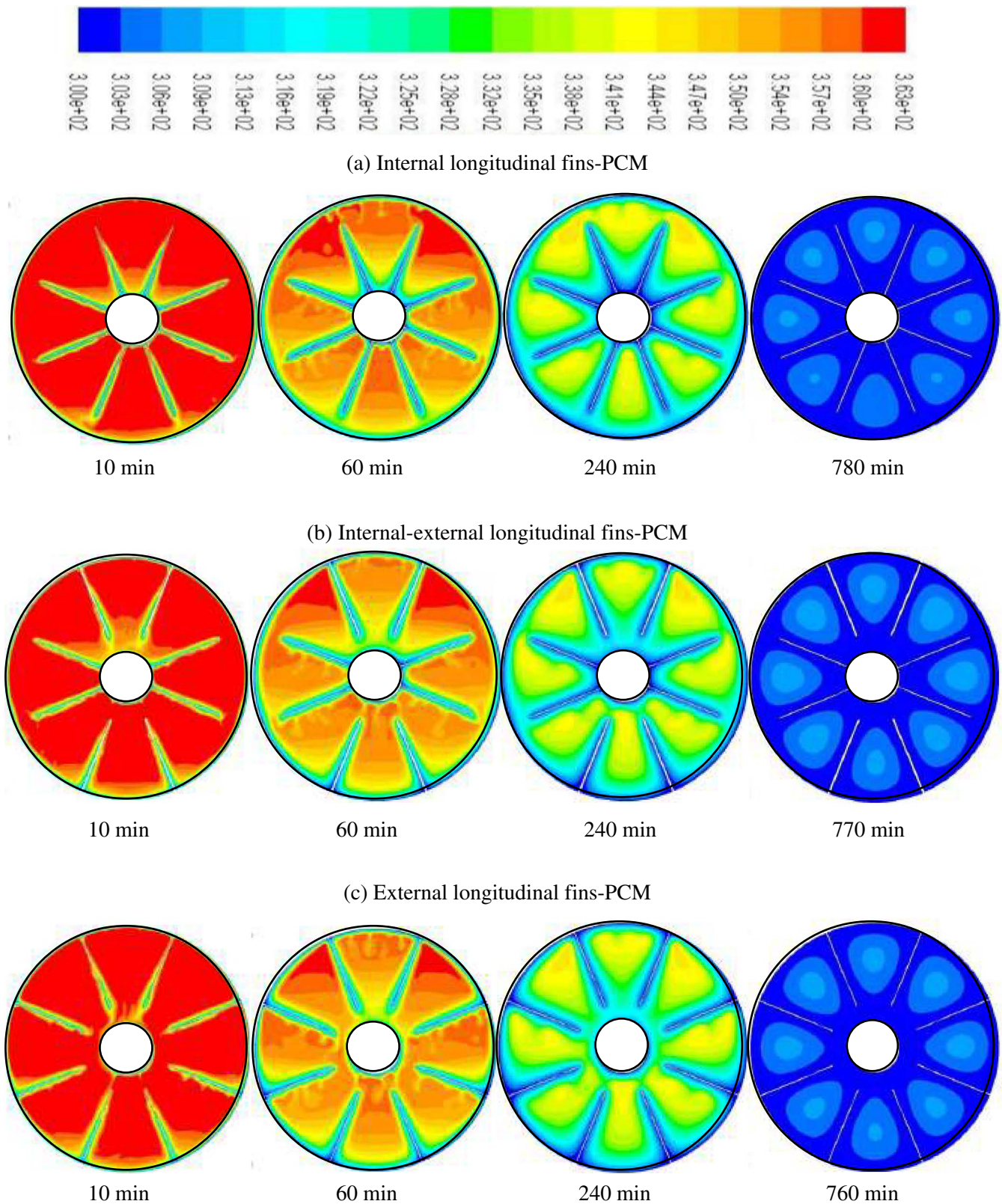


Fig. 12. Liquid fraction contours in the TTHX obtained using longitudinal fins-PCM technique.

4.1.4. Axial and angular temperature variations for PCM-TTHX

As illustrated in Fig. 1, four T-type thermocouples inserted in the PCM, and each one has four sensors. Two thermocouples on the top and bottom of the storage tank were fitted in the axial direction positioned at (A = 500 mm and B = 1100 mm) from the HTF-tube entrance. Fig. 9

shows the average temperature variations in the axial direction for both-sides freezing method at average discharging temperature of 65 °C. The temperature variation was linear for the sensible cooling period. A significant variation on the solidification of PCM has been seen during discharging process at positions A and B from the entrance

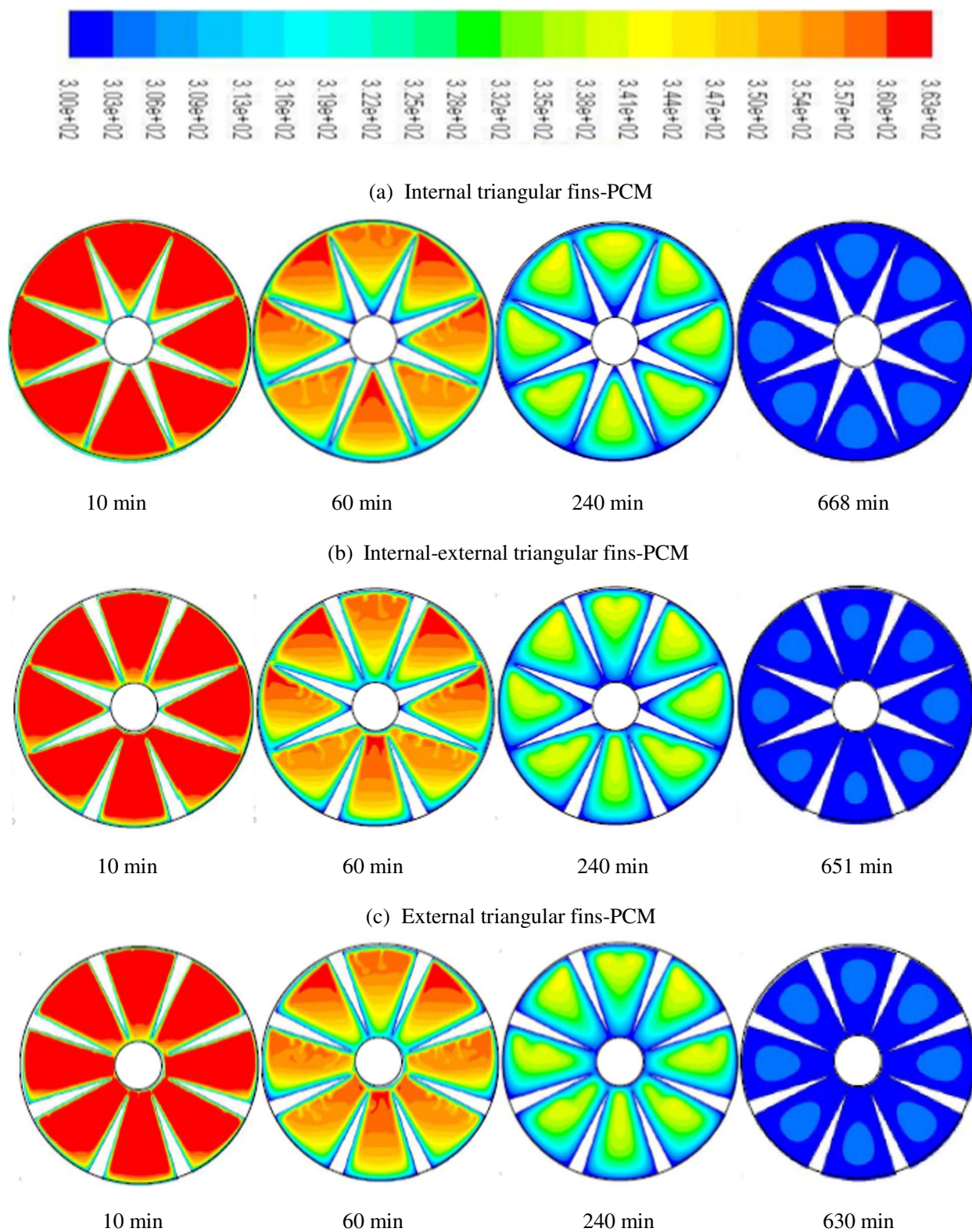


Fig. 13. Liquid fraction contours in the TTHX obtained using triangular fins-PCM technique.

of the HTF-tube because of the disturbance in the flow rate at the entrance, as the large internal pipes diameter were changed from 76.2 mm to 500 mm. Therefore, the PCM solidification completed, as fast as at position B than position A of the TTHX in the axial direction.

Fig. 10 also shows the average temperature variations along the angular direction for both-sides freezing method at $T_i = 65^\circ\text{C}$. The solidification rate decreased, as the angle direction increased from

$\theta = 90^\circ$ to $\theta = 270^\circ$ because of the cooling rate at the upper tube was higher than the lower tube. Therefore, the solid layer can be fully seen on the top of tube, as fast as on the bottom of same tube.

4.1.5. Thermodynamic analysis of discharging process

Fig. 11 presents the inlet and outlet discharging temperatures of the HTF, as well as the average temperature of the PCM versus the time for

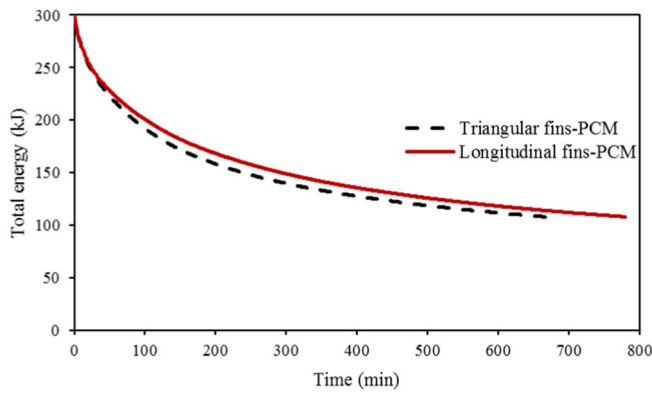


Fig. 14. The total energy released for solidifying the PCM in TTHX-longitudinal and TTHX- triangular fins.

Table 4 The melting fraction and total energy released of the PCM in TTHX.

Time (min)	Melting fraction		Total released energy (kJ)	
	PCM-longitudinal	PCM-triangular	PCM-longitudinal	PCM-triangular
30	0.810629964	0.798801184	243.9165156	240.9688281
120	0.558027983	0.513505876	192.3173906	182.9887344
240	0.395805806	0.348748446	159.6270313	149.8864844
440	0.256435037	0.21936138	131.378375	123.7634922

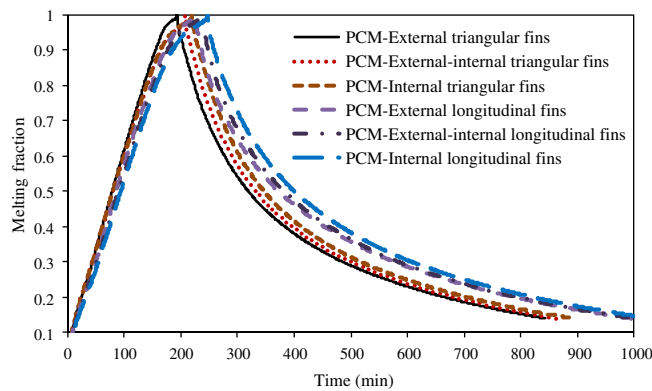


Fig. 15. The PCM melting and solidification time durations for all longitudinal/triangular fins case in the TTHX.

the TTHX with internal longitudinal fins during the freezing process. The discharging temperature of the PCM solidification was at 65 °C with a flow rate of 37.5 kg/min. It can be seen for the solidification tests, the PCM temperature decreased rapidly initially during the sensible cooling period of these process. As the phase transitions started, the difference between the inlet and outlet discharging temperatures was decreased for a long time, until the PCM solidification was completed.

4.2. Uncertainty analysis

The uncertainty of a measured quantity is an error of measurement analysis for showing the level of confidence of the experimental results. The uncertainty of PCM thermal properties, such as the onset point, peak point, and latent heat of fusion during heating and freezing process can be split into two components, namely: random and systematic components of uncertainty. Random components of uncertainties are the standard error that can be analyzed statistically by determining the mean and by calculating the standard deviation for a finite set of measurements. In this study, some measurements were eliminated from

the set based on the Chauvenet's criterion to reject certain measurement [21]. A new mean and standard deviation were determined based on the modified measurement set. Table 3 summarizes the new mean and the standard uncertainties of the PCM thermal measurement with (confidence interval 90%) of the PCM thermal properties.

4.3. Numerical results

4.3.1. Heat-transfer enhancement of the PCM solidification with longitudinal fins

The liquid fraction contours of the PCM in a TTHX with a various configuration of longitudinal fins at different times are shown in Fig. 12. First, heat-transfer occurred between the cold wall of the tube and the liquid surface of the PCM via conduction, which dominated the solidification process at the early stage and caused a very thin layer of the solid to surround the longitudinal fin surface and the cold wall of the tube, while the rest of the PCM remained liquid without any phase-change because the effects of the natural convection controlled heat-transfer mechanism were limited. After 10 min, small convection cells created between the walls of the fins and subsequently expanded to the middle tube. Over time, convection cells emerged and large convection cells were formed at 60 min. The solid fraction expanded to the bottom part of the tube at 240 min because of natural convection effects driven by buoyancy, and the solid part of the PCM was squeezed because of its high density. The solid fraction was increased in all directions of the tube with time. The PCM was entirely solidified at 780, 770, and 760 min for internal, internal-external, and external longitudinal fins, respectively.

4.3.2. Heat-transfer enhancement of the PCM solidification with triangular fins

The thermal behaviors of liquid fraction that occurred for the PCM in TTHX-longitudinal fins were same for TTHX-triangular fins configuration. Nevertheless, the difference in solidification times were 668, 651, and 630 min for internal, internal-external, and external triangular fins respectively, as shown in Fig. 13.

During the freezing process for the aforementioned PCM in the TTHX-longitudinal and TTHX-triangular fins configuration, the cold-water flows through both the inner and outer tubes, the PCM temperature decreased until reaches the freezing temperature at 65 °C, the PCM gradually solidifies in the middle tube and releases heat, where the PCM solid at from the wall of the longitudinal/triangular fins was higher than that at the upper or lower part of the middle tube. Because of the large difference between the HTF and PCM temperatures. However, the thickness of solid layer was increased and filled the gaps between the fins wall and closed to the middle tube to provide thermal conduction resistance that decreased the heat-transfer rate. Hence, the discharging time was gradually decreased until the PCM was entirely solidified. The natural convection influence resulted in a uniform temperature distribution in the molten PCM and prevented the container material from overheating. Consequently, the employment of the fins in a different configuration is more necessary for improving the solidification rate.

4.3.3. Total energy released for PCM-fins

Fig. 14 shows the total energy released for the PCM in TTHX-longitudinal and TTHX-triangular fins simulated using Fluent 15 software at different times of the both-sides freezing process. PCM-triangular fins for the internal fins configuration has lower energy released, compared with the same PCM volume with internal longitudinal fins. However, Table 4 shows that the melting fraction values for PCM-longitudinal fins were higher than those of the PCM-triangular fins model. Consequently, the energy released rate by triangular fins takes shorter time than longitudinal fins. The PCM-triangular fins model exhibits effective energy released because of the enhancement in heat-transfer by fins.

4.4. Comparison of solidification time for all cases

After the PCM entirely melted, the solidification process starts [6]. Fig. 15 shows the PCM melting and solidification time durations for all longitudinal/triangular fins case used in the TTHX. A significant enhancement can be observed for the PCM solidification time using internal, internal-external and external triangular fins at 14%, 16%, and 18% respectively, compared to the PCM-longitudinal fins configuration. Furthermore, the solidification time was decreased after using external triangular fins to 6% and 3%, internal and internal-external triangular compared to fins, respectively. The solidification retardation was decreased much more with triangular fins because the effect of cooling rate was larger for triangular fins than that of the longitudinal fins in the TTHX. Consequently, the model of the external triangular fins was welded into the middle tube of TTHX considered to be the most efficient technique to accomplish the shorter time for solidifying the PCM at 630 min.

5. Conclusions

The heat-transfer enhancement to PCM that was successfully solidified in a large TTHX by two types of extended surfaces, namely: longitudinal and triangular fins, was investigated. The both-sides freezing was the main method used in this study at average discharging temperature of 65 °C. The influence of mass flow rate on these process in the axial direction was investigated based on the change in mass flow rate of 16.2, 29.4, and 37.4 min/kg. The solidification rate increased, as the mass flow rate increased with the heat-transfer enhancement by internal longitudinal fins. A significant temperature variation for axial and angular direction has been observed during discharging process, which caused the PCM solidification completed, as fast as at position B than position A from the entrance of the HTF-tube of the TTHX. Also, a significant enhancement on solidification time was achieved using internal, internal-external, and external triangular fins at 14%, 16%, and 18%, respectively, compared with the configurations employing longitudinal fins. Consequently, the most efficient configuration for solidifying the PCM is the external triangular finned-tube (630 min), where the solidification time was decreased to 6% and 3%, internal and internal-external triangular compared to fins, respectively. Furthermore, the total energy released for the PCM in TTHX-longitudinal and TTHX-triangular fins were compared. The numerical results for the both types of fins were confirmed by the close agreement with the experimental results of the PCM in TTHX-internal longitudinal fins.

Nomenclature

C	mushy zone constant (kg/m ³ s)
C_p	specific heat (J/kg K)
g	gravity acceleration (m/s ²)
h	sensible enthalpy (J/kg)
H	enthalpy (J)
HTF	heat-transfer fluid
k	thermal conductivity (W/m K)
L	latent heat of fusion (J/kg)
LHTES	latent heat thermal energy storage
p	pressure (Pa)
PCM	phase-change material
r	tube radius (mm)
S	momentum source term (Pa/m)
t	time (min)
T	temperature (°C or K)
TTHX	triplex-tube heat exchanger
T_m	melting temperature (°C or K)
u	velocity component (m/s)
v	velocity component (m/s)
x, y	x, y -component in a cartesian coordinate system

Greek letters

β	thermal expansion coefficient (1/K)
ε	constant
γ	liquid fraction
μ	dynamic viscosity (kg/m s)
θ	angle (°)
ρ	fluid density (kg/m ³)

Subscripts

i	inner
ini	initial time
l	liquid PCM
m	middle
o	outer
pcm	phase-change material
ref	reference
s	solid PCM

Acknowledgements

The authors gratefully appreciate the financial supports provided by Solar Energy Research Institute (SERI), Universiti Kebangsaan Malaysia (UKM) (K005520), Malaysia.

References

- [1] S. Jegadheeswaran, S.D. Pohekar, Performance enhancement in latent heat thermal storage system: a review, *Renew. Sust. Energ. Rev.* 13 (2009) 2225–2244.
- [2] H. Niyas, P. Muthukumar, Performance analysis of latent heat storage systems, *Int. J. Scient. Eng. Res.* 4 (2013) 2229–5518.
- [3] Y.L. Jian, Numerical and experimental investigation for heat transfer in triplex concentric tube with phase change material for thermal energy storage, *Sol. Energy* 82 (2008) 977–985.
- [4] A.M. Abdulateef, S. Mat, J. Abdulateef, K. Sopian, A.A. Al-Abidi, Geometric and design parameters of fins employed for enhancing thermal energy storage systems: a review, *Renew. Sust. Energ. Rev.* 82 (2018) 1620–1635.
- [5] F. Agyenim, P. Eames, M. Smyth, A comparison of heat transfer enhancement in a medium temperature thermal energy storage heat exchanger using fins, *Sol. Energy* 83 (2009) 1509–1520.
- [6] A.M. Abdulateef, S. Mat, K. Sopian, J. Abdulateef, A.A. Gitan, Experimental and computational study of melting phase-change material in a triplex tube heat exchanger with longitudinal/triangular fins, *Sol. Energy* 155 (2017) 142–153.
- [7] N.H.S. Tay, F. Bruno, M. Belusko, Comparison of pinned and finned tubes in a phase change thermal energy storage system using CFD, *Appl. Energy* 104 (2013) 79–86.
- [8] K.R. Manish, B. Jyotirmay, Thermal performance enhancement of shell and tube latent heat storage unit using longitudinal fins, *Appl. Therm. Eng.* 75 (2015) 1084–1092.
- [9] G.R. Solomon, R. Velraj, Analysis of the heat transfer mechanisms during energy storage in a phase change material filled vertical finned cylindrical unit for free cooling application, *Energy Convers. Manag.* 75 (2013) 466–473.
- [10] A. Castell, C. Sole, M. Medrano, J. Roca, L.F. Cabeza, D. Garcia, Natural convection heat transfer coefficients in phase change material (PCM) modules with external vertical fins, *Appl. Therm. Eng.* 28 (2008) 1676–1686.
- [11] A.C. Celador, G. Diarce, I.G. Pino, J.M. Sala, Development and comparative analysis of the modeling of an innovative finned-plate latent heat thermal energy storage system, *Energy* 58 (2013) 438–447.
- [12] A. Sciacovelli, F. Gagliardi, V. Verda, Maximization of performance of a PCM latent heat storage system with innovative fins, *Appl. Energy* 137 (2015) 707–715.
- [13] M. Akgun, O. Aydin, K. Kaygusuz, Thermal energy storage performance of paraffin in a novel tube-in-shell system, *Appl. Therm. Eng.* 28 (2008) 405–413.
- [14] A.A. Al-Abidi, S. Mat, K. Sopian, M.Y. Sulaiman, A.T. Mohammad, Experimental study of melting and solidification of PCM in a triplex tube heat exchanger with fins, *Energy Build.* 68 (2014) 33–41.
- [15] A.A.R. Darzi, M. Farhadi, K. Sedighi, Numerical study of melting inside concentric and eccentric horizontal annulus, *Appl. Math. Model.* 36 (2012) 4080–4086.
- [16] A.D. Brent, V.R. Voller, K.J. Reid, Enthalpy-porosity technique for melting convection-diffusion phase change: application to the melting of a pure metal, *Numer. Heat Transf.* 13 (2007) 297–318.
- [17] C. Guo, W. Zhang, Numerical simulation and parametric study on new type of high temperature latent heat thermal energy storage system, *Energy Convers. Manag.* 49 (2008) 919–927.
- [18] M.J. Hosseini, A.A. Ranjbar, K. Sedighi, M. Rahimi, A combined experimental and computational study on the melting behavior of a medium temperature phase change storage material inside shell and tube heat exchanger, *Int. Commun. Heat Mass Transf.* 39 (2012) 1416–1424.

- [19] S.V. Patankar, *Numerical Heat Transfer and Fluid Flow*, McGraw Hill, New York, 1980.
- [20] A.A. Al-Abidi, S. Mat, K. Sopian, M.Y. Sulaiman, A.T. Mohammad, CFD applications for latent heat thermal energy storage: review, *Renew. Sust. Energ. Rev.* 20 (2013) 353–363.
- [21] J.P. Holman, *Experimental Methods for Engineers*, McGraw Hill, New York, 2012.